Surface-Enhanced Raman Spectroscopy of Carbon Electrode Surfaces Following Silver Electrodeposition

Yang Wang Alsmeyer and Richard L. McCreery*

Department of Chemistry, The Ohio State University, 120 W. 18th Avenue, Columbus, Ohio 43210

Electrodeposition of Ag particles on glassy carbon (GC) resulted in up to a 100-fold enhancement of Raman scattering from the carbon substrate. The enhancement was a maximum when 0.21 μmol/cm² of Ag was deposited and was greater when small (~400-Å) Ag particles were present. Although the enhancement of carbon scattering was large, it was fragile, decaying with time after Ag deposition. On the basis of surface-enhanced Raman theory, the sampling depth of the enhanced spectra is approximately 20 Å, compared to ca 250 Å for conventional Raman of GC. SERS spectra of GC and pyrolytic graphite (PG) exhibited a stronger "disorder" band, either because the method is more surface selective or because the Ag preferentially deposits on electrochemically active surface defects. The approach was used to examine cleaved and laser-activated PG surfaces and polished highly oriented PG (HOPG), and it was demonstrated that laser damage is more extensive on the surface than the normal Raman spectrum implies.

INTRODUCTION

The wide variety of surface preparation procedures for carbon electrodes leads to quite variable electrochemical performance (*1–3*). Electron-transfer rates, adsorption, and background current all depend strongly on surface history, with variations of several orders of magnitude in k^0 being observed even for allegedly simple redox systems (*4–13*). While a comprehensive understanding of the variables that affect electrode kinetics on carbon is not yet available, it is clear that surface cleanliness and carbon microstructure are of major importance. Unfortunately, the process of relating surface structure to electron-transfer activity has been hindered by the lack of adequate probes of carbon surface structure at the molecular level. Without such probes, conclusions about surface pretreatment effects on electrochemical behavior are necessarily indirect and provide limited structural insight.

In several previous reports, we discussed the relationship between the Raman spectra of carbon materials and their electron-transfer activity (*13–15*). A correlation between the 1360-cm^{-1} "disorder" (D) band of carbon and electron-transfer kinetics for $Fe(CN)_6^{3-/4-}$ and dopamine was noted, indicating that graphitic edges associated with disorder are important to fast electron transfer. Through correlation of k^0 for $Fe(CN)_6^{3-/4-}$ with capacitance and D band intensity, it was possible to hypothesize that the electron-transfer rate is directly proportional to the surface fractional edge plane density, f_e (*15*). Thus, the Raman spectrum of carbon electrodes provides structural information on at least one of the surface variables that determine k^0 on carbon electrodes.

Although conventional Raman spectroscopy has been a very useful probe of carbon structure, it should be recognized that the sampling depth is significantly greater than UHV surface analytical techniques such as Auger and XPS. The photon penetration and escape depths for Raman are usually greater than the electron escape depths relevant to XPS and Auger, leading to lower surface selectivity for the optical probe. For carbon probed with a visible laser at normal incidence, the sampling depth is ca. 300 Å (*3*) and should be somewhat less at non-normal incidence. Although this sampling depth is fairly small due to the opacity of carbon, it is still large compared to the electrochemically relevant depths of a few tens of angstroms. Thus, a pretreatment procedure that affects only a few atomic layers of a carbon surface may not be detected by a normal Raman probe due to a relatively large signal from the several hundred anstroms of bulk carbon.

The current work was initiated to decrease the effective sampling depth of Raman spectroscopy by exploiting the surface enhanced Raman effect (SERS). Although SERS has been studied extensively because of its high sensitivity and surface selectivity (*16*), the vast majority of work has been carried out on Ag, Au, and Cu substrates. Carbon itself is not a suitable SERS substrate due to its unsuitable optical and electronic properties, and any enhancement on carbon would be very small. In order to exploit SERS for examining carbon materials, we used an approach that is similar to that of Pemberton (*17*) in which small, SERS active Ag particles were electrodeposited on Pt surfaces. As was observed for vapor-deposited Ag particles (*18–20*), the material near the Ag particles exhibited enhanced Raman due to the electromagnetic field enhancement by the Ag. Thus, the carbon electrode material near an electrodeposited Ag particle of suitable size should exhibit enhanced Raman within a few tens of angstroms of the Ag (*16b*, *20*). Since such Raman enhancement distances are much less than the 300-Å normal Raman sampling depth, the SERS technique should be more surface selective than conventional Raman. In this paper, we will discuss the deposition technique, enhanced spectroscopy, and applications to several carbon electrodes.

EXPERIMENTAL SECTION

A schematic diagram of the instrument is shown in Figure 1. The spectrometer and collection optics have been described previously (*21*), and the band reject (Pomfret optics, Orange, VA) and band-pass (Oriel) filters were both centered on the 514.5-nm laser line. The cell was designed both to hold a variety of electrode materials and to properly orient the incident beam, electrode surface, and collection optics. The beam impinged on the electrode at an angle of 75 ± 5° to the surface normal with the polarization parallel to the electrode surface. An Ag wire quasi-reference electrode (QRE) and Pt auxiliary electrode were inserted in the solution out of the optical path at opposite sides of the cell. The working electrode is shown in Figure 2. Teflon plumber's tape was used to seal the holder to the carbon electrode material. It was important to avoid strain on the carbon during mounting, particularly for graphite samples, so the soft Teflon tape gasket was preferable to an O-ring.

Coarse optical alignment was carried out with a dummy glassy carbon (GC) electrode positioned in the cell with solution present. Laser scatter was strong enough from GC to permit orientation of the electrode and incident beam such that the scattered light was imaged on the entrance slit. Then the electrode position and collection lens were adjusted to maximize the D band intensity for a Raman spectrum of the GC. It was important to have solution present to produce the same focusing conditions present during the experiment. Once an adequate signal from the dummy

* Author to whom correspondence should be addressed.

0003-2700/91/0363-1289$02.50/0

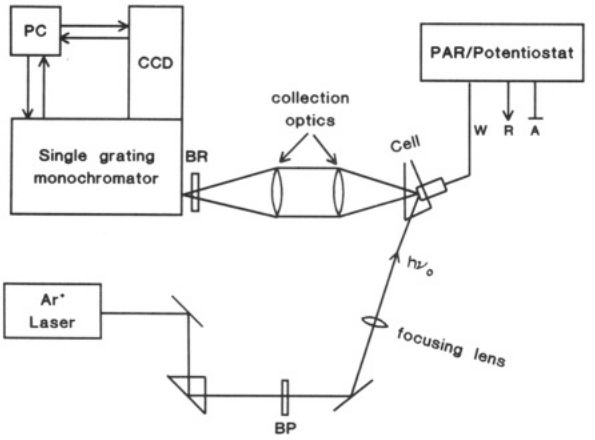

Figure 1. Schematic diagram of the experimental apparatus. Reference and auxiliary electrodes were placed on opposite sides of the working electrode. BR and BP are band reject and band-pass filters. Laser power at sample was ~10 mW, entrance slit width was 125 μm.

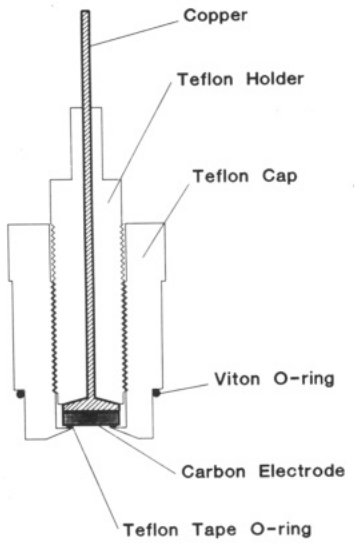

Figure 2. Detail of electrode holder. Entire assembly could be removed from cell without major disturbance of optical alignment. Teflon tape seal minimized pressure on carbon sample.

GC electrode was obtained, the GC was replaced with the electrode to be studied. The cell design permitted removal and replacement of the working electrode assembly with minimal disturbance to its position. With the new electrode in place, the Raman intensity was again maximized on the D band for GC or the E_{2g} band for pyrolytic graphite (PG) or highly oriented PG (HOPG).

After significant trial and error, the optimum Ag deposition conditions for maximum SERS intensity were determined. The solution was 0.5 mM $AgNO_3$ plus 0.1 M $NaClO_4$ or 0.1 M $NaNO_3$ in Nanopure (Barnstead) water. In this medium, the Ag wire QRE had a potential of 0.332 V vs SCE. The QRE was preferable to a conventional reference electrode because of lack of contaminants, particularly chloride ion. Constant current from a PAR 173 galvanostat was used to deposit Ag, in order to easily control the total amount deposited. For a current of 20 μA on a 0.12–0.38 cm^2 electrode area, the deposition potential ranged from –0.4 to –0.6 V vs QRE. Larger current densities resulted in more negative potential excursions and were avoided. Deposition times were varied as described below but were typically 1–5 min. Carbon materials were Tokai GC-20 glassy carbon, pyrolytic graphite from Pfizer, and HOPG from Union Carbide (ungraded material from Arthur Moore).

The spectrometer shown in Figure 1 is a modification of a previous design (*21*). A 200 line/mm grating in the ISA 640 spectrograph operated in second order produced a ca. 800-cm^{-1} Raman shift range when centered at 1340 cm^{-1} relative to the 514.5-nm Ar^+ laser. The detector was a 1-cm × 1-cm CCD, which

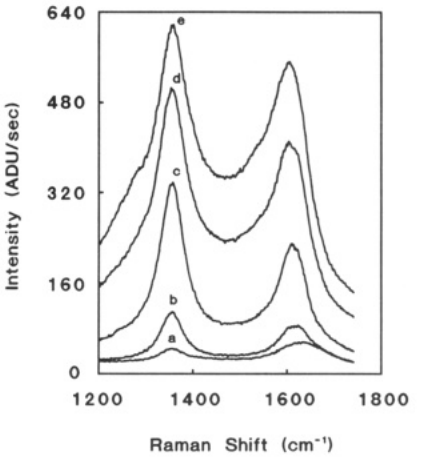

Figure 3. Raman spectra of polished GC-20 before and during Ag deposition. 5-s CCD integration times, laser off during deposition. Spectrum a is of the initial GC surface in solution but before deposition. Curves b–e are after Ag deposition as follows: b, 0.041 μmol/cm^2; c, 0.099 μmol/cm^2; d, 0.145 μmol/cm^2; e, 0.248 μmol/cm^2.

was binned to become a 512 × 1 detector. Laser power at the sample surface was 10 MW on a 50-μm × 2-mm focal spot. The laser light was kept off except during spectrum acquisition to minimize any photodegradation effects during deposition and observation. The beam waist at the electrode was relatively wide, ~50 μm, thus keeping the power density relatively low. The typical CCD integration time was 5 s, with neglible dark counts for the CCD cooled to –110 °C. The Raman shift range was calibrated with a neon lamp each time the grating was repositioned. Intensities are expressed as CCD analog/digital converter units per second of integration, with each A/D unit corresponding to approximately 15 photoelectrons.

The overall experimental sequence was as follows: the cell and dummy GC electrode were aligned relative to the laser and spectrometer in the presence of solution, using both elastic scatter (crude alignment) and the carbon Raman bands (fine tuning). The GC electrode was replaced with the test electrode, and the alignment was fine tuned. Once alignment was complete, an initial spectrum was obtained (5-s integration time). With the laser off, Ag was deposited with constant current until the desired average film thickness was achieved. The working electrode was disconnected, the laser turned on, and the spectrum acquired immediately. Successive spectra at various Ag thicknesses were often obtained, with the laser on only during spectrum acquisition.

RESULTS

Raman spectra obtained before and after Ag deposition on conventionally polished GC are shown in Figure 3. The peak intensities increase by factors of up to 100 upon deposition, depending on Ag coverage. The integrated intensity ratio of the D to E_{2g} bands increases from 1.25 to a maximum of 2.0 upon Ag deposition. The changes in shape of the E_{2g} peak at ~1600 cm^{-1} are due mainly to interference by water in the initial spectrum. Once the SERS intensity becomes large, the H_2O signal becomes insignificant compared to the carbon E_{2g} band. The absolute D band intensity (1360 cm^{-1}) and baseline are compared in Figure 4 as functions of Ag deposition time. For the polished GC surface, the maximum SERS intensity is reached at an average Ag coverage of 2.1×10^{-7} mol/cm^2, based on the geometric electrode area.

SEM's of the polished GC surface are shown in Figure 5A–D at two coverages and magnifications. On low magnification (A and C), a distribution of "large" Ag particles with diameters of ca. 2500 Å is apparent, plus numerous smaller particles visible upon close inspection. Higher magnification (B and D) reveals numerous particles in the 100–1000-Å range, with a higher density of small particles for the higher Ag coverage. As shown in Figure 5E, Ag on freshly cleaved HOPG leads to relatively large particles and clusters of ca. 1000-Å particles

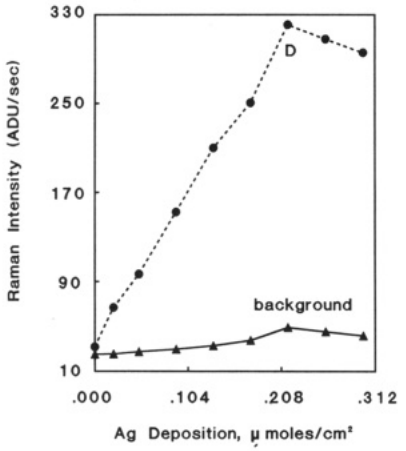

Figure 4. Raman intensities of D band (1354 cm^{-1}) and baseline during Ag deposition.

but few isolated small particles. In Figure 5F, a high density of small Ag particles is apparent on mechanically damaged regions of polished HOPG.

As shown in Figures 6 and 7, the SERS signal decays with time, whether or not the laser is on continuously. Although the signal degradation can be serious on a several minute time scale, the spectra are strong enough and the CCD fast enough to obtain excellent spectra in 5 s after deposition. Furthermore, the reproducibility of signal strength is fairly poor, with peak intensities having a standard deviation of 50% for N = 10. Thus, quantitative conclusions based on absolute intensity will be difficult in any case, and the signal decay must be considered in the experimental design.

Although the polished GC surfaces used for Figures 3–7 demonstrate that SERS can be used to enhance substrate scattering, structural inferences are more straightforward with more ordered HOPG samples. Raw spectra obtained from HOPG, which was lightly polished with 0.05-μm alumina, are shown in Figure 8. The E_{2g} band at 1582 cm^{-1} is the only graphite feature visible above the H_2O background before Ag deposition. As Ag is deposited, the D and E_{2g} bands become prominent, and the D/E_{2g} intensity ratio increases. The trend is more clear after the water background is subtracted, as in Figure 9. The D band is not apparent before Ag deposition but is prominent after 3.6×10^{-8}–2.5×10^{-7} mol/cm^2 of Ag has been deposited. On the basis of an equivalent monolayer coverage of ca 350 $\mu C/cm^2$ (*17*, *22*) or 3.6×10^{-9} mol/cm^2, the SERS effect begins at 10 average monolayers and is most prominent for 70 average monolayers of Ag. The integrated

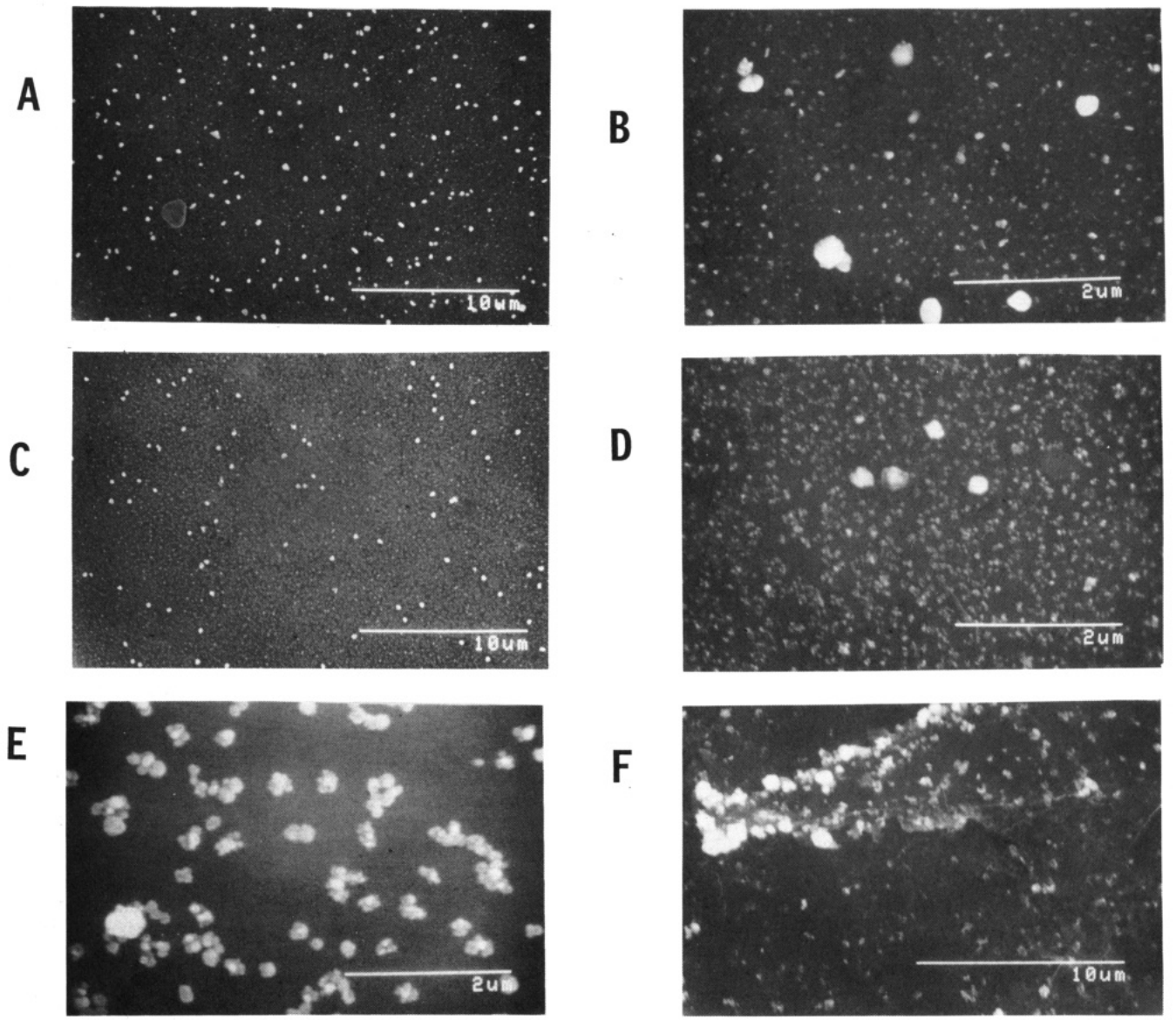

Figure 5. SEM's of GC (A–D) and HOPG (E, F) surfaces after Ag deposition. A and B are after 0.04 μmol/cm^2 C and D after 0.12 μmol/cm^2. E was obtained after Ag deposition on freshly cleaved HOPG and F after deposition on lightly polished HOPG.

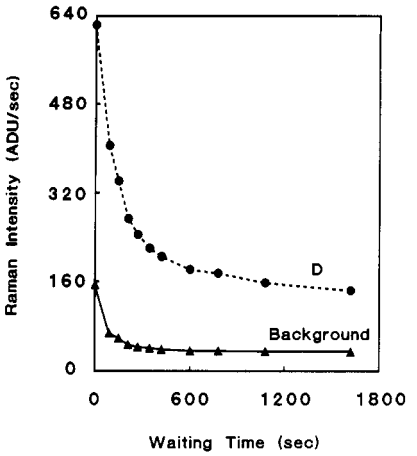

Figure 6. Decay of the D band and background Raman signals with time after Ag deposition was completed. Electrode remained in solution with laser on continuously. Initial Ag coverage was 0.24 μmol/cm^2.

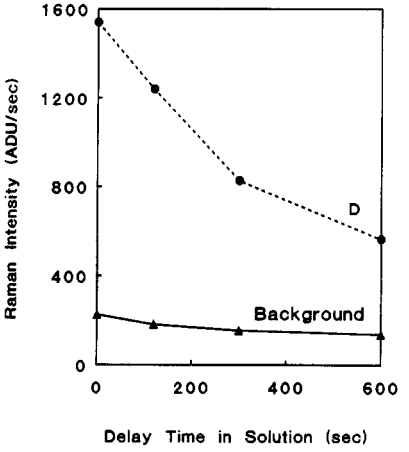

Figure 7. Decay of Raman intensity with time after Ag deposition. Conditions same as Figure 6, but Ar^+ laser was turned off between spectra.

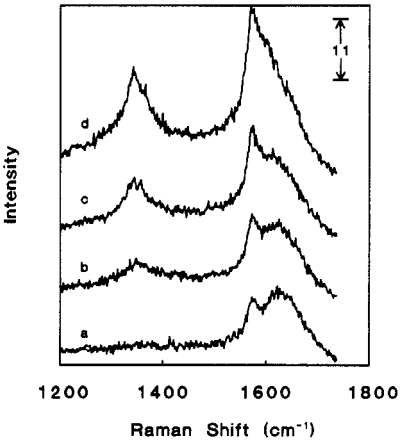

Figure 8. In situ Raman spectra of lightly polished HOPG before and after Ag deposition. Scale indicates ADU/s for all four spectra. Spectrum a, 0 μmol/cm^2 of Ag; b, 0.041 μmol/cm^2; c, 0.12 μmol/cm^2; d, 0.25 μmol/cm^2.

D/E_{2g} intensity increases from near 0 to 0.73 upon Ag deposition. Not only is the D/E_{2g} intensity ratio much higher after Ag deposition, but there is also a shoulder on the high-frequency side at the E_{2g} mode, a feature associated with delamination of the graphite and increased d_{002} spacing (*13*).

As noted earlier, enhanced Raman scattering was not observed following Ag deposition on cleaved HOPG, apparently because the particle size is unsuitable for SERS. However,

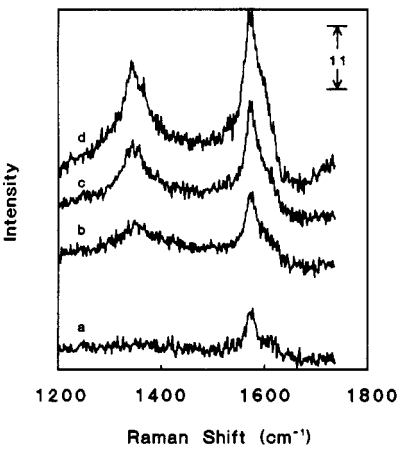

Figure 9. Same as Figure 8 but with H_2O background subtracted.

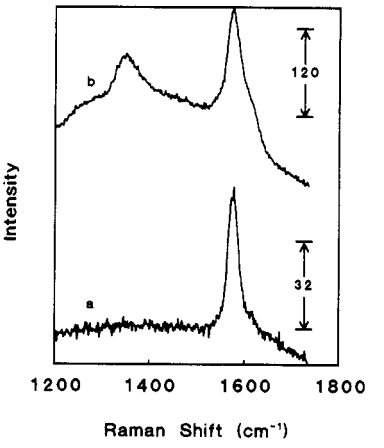

Figure 10. Raman spectra of cleaved PG basal plane. PG was cleaved in solution, and both spectra are corrected for H_2O background. Scale indicates ADU/s for each spectrum. Spectrum a is before Ag deposition, b is after 0.41 μmol/cm^2 of Ag was electrodeposited.

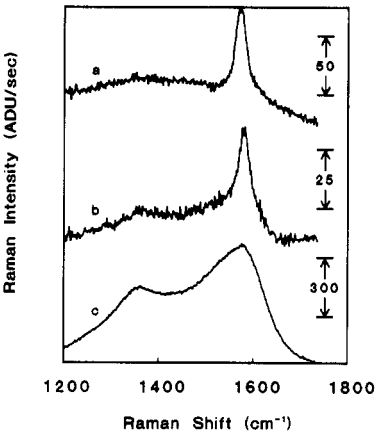

Figure 11. Raman spectra of cleaved PG, with relative scales indicated in ADU/s. Spectrum a is cleaved basal plane before Ag deposition. Spectrum b is same surface after three 50 MW/cm^2 Nd:YAG pulses were delivered in air. Spectrum C is the surface of curve b following deposition of 0.12 μmol/cm^2 of Ag.

pyrolytic graphite (PG) is similar to HOPG except it is not subjected to the final pressure annealing. It is less ordered than HOPG, with smaller microcrystallite sizes, but retains the macroscopic and microscopic layered structure. Figure 10 shows Raman spectra of the freshly cleaved basal plane of PG before and after Ag deposition. Unlike the data of Figures 8 and 9, the PG surface was not scratched or pretreated in any way. The D band is unobservable in the normal

Raman spectrum but increases in intensity upon Ag deposition. Figure 11 shows the effect of pulsed Nd:YAG laser irradiation on the PG spectrum. Laser treatment without Ag deposition causes a slight increase in D band intensity, sufficient to elevate the band above background. Following Ag deposition, the D band is much stronger, and the spectrum is similar to that for quite disordered sp^2 carbon. As with earlier experiments, Ag deposition greatly increases the absolute Raman intensities.

As noted in the Introduction, the surface selectivity of Raman scattering will be dependent on effective sampling depth. The normal Raman sampling depth may be estimated from the optical properties of GC and HOPG, using a modification of the approach of Wada and Solin (*23*) and Loudon (*24*, *25*). The observed Raman signal at a particular sample depth, $R(z)$, will be related to the local laser intensity as it penetrates the solid, $I_L(z)$, and the attenuation of Raman scattering intensity as it leaves the solid. Therefore, the observed Raman sampling depth will be significantly smaller than the laser penetration depth. At normal incidence,

$$I_L(z) = I_0(1 - r)e^{-4\pi k_L(z/\lambda_L)} \quad (1)$$

$$R(z) = \gamma I_L(z)e^{-4\pi k_R(z/\lambda_R)} \quad (2)$$

where I_0 is the incident laser intensity, z the sample depth, and γ a constant incorporating the Raman scattering cross section, number density, etc. k_R and k_L are the absorption coefficients of the carbon at the Raman and laser photon wavelengths, λ_R and λ_L, and r is the reflectivity. After approximating that the scattered and laser wavelength are sufficiently close to each other to equate, the normal incidence Raman signal at a particular z becomes

$$R(z) = I_0(1 - r)\gamma e^{-8\pi k_L(z/\lambda_L)} \quad (3)$$

The total observed Raman scattering is proportional to the integral of eq 3 over the depth variable z. We will arbitrarily define the sampling depth, z_{63}, as the sample thickness that will generate 63% $(1 - e^{-1})$ of the Raman signal observed for a sample of infinite thickness. Integration of (3) leads to

$$S(z) = S_{max}(1 - e^{-8\pi k_L(z/\lambda_L)}) \quad (4)$$

$$S_{max} = \frac{I_0(1 - r)\gamma\lambda_L}{8\pi k_L} \quad (5)$$

where $S(z)$ indicates the total Raman signal for a sample of thickness z. Setting $S(z)/S_{max} = 1 - e^{-1}$ permits determination of z_{63} for normal incidence:

$$z_{63} = \frac{\lambda_L}{8\pi k_L} \quad (6)$$

For GC with a 515-nm laser at normal incidence ($k_L = 0.70$) (*26*), z_{63} is 291 Å, while for the HOPG basal plane ($k_L = 1.52$ at 515 nm) (*23*), z_{63} is 135 Å. Thus, 63% of the total Raman signal for GC at normal incidence is derived from the carbon within 290 Å of the surface (*3*). Obviously the sampling depth varies with λ_L and to a much smaller degree on the Raman shift, $\Delta\bar{\nu}$.

For the geometry of Figure 1, with non-normal laser incidence and near-normal collection optics, the situation is more complex. $I_L(z)$ will vary with the incident angle, θ_i, and this dependence was predicted by using classical treatments (*27*). $I_L(z)$ was calculated by using the transmittance of a thin carbon film for light polarized parallel to the electrode surface. The "thick film" model (eq 27 in ref 27) was used to avoid any interference effects, and the film thickness was gradually increased to calculate I_L as a function of z. The resulting $I_L(z)$ curve was substituted into eq 2 and z_{63} was determined by numerical integration. The results are shown in Table I, along with the calculated reflectivity. In all cases, the electrode was assumed to be immersed in water ($n = 1.33$). The calculation was compared to one based on the mean-square electric field predictions of Porter et al. (*28*) to calculate $I_L(z)$, with identical results.

Table I. Calculated Reflectivity and Raman Sampling Depth

θ_i	reflectivity[b]	z_{63},[c] Å
Glassy Carbon (n = 1.79, k = 0.70,[a] λ_L = 515 nm)		
0°	0.0688	291
30	0.0997	281
45	0.1493	270
60	0.2612	260
75	0.5004	252
85	0.7924	250
89	0.9545	250
HOPG (n = 1.79, k = 1.52,[d] λ_L = 515 nm)		
0	0.2093	135
75	0.6820	125

[a] From ref 26. [b] Sample immersed in water (n = 1.33) in all cases. [c] Sample depth yielding 63% of maximum Raman signal. [d] Calculated from ref 23.

DISCUSSION

Considering the normal Raman experiment first, several useful observations are available from the results. The effective sampling depth z_{63} is 250–300 Å for GC, and is weakly dependent on the angle of incidence. Although surface selectivity can be improved somewhat at glancing incidence over normal incidence, the sampling depth still exceeds 200 Å. It should be noted that z_{63} decreases with decreasing λ_L and is smaller for the more strongly absorbing HOPG. The reflectivity is strongly θ_i dependent, with higher angles of incidence coupling significantly less light into the solid sample and reflecting more. At the 75° angle employed in the current experiments, 50% of the laser light enters the GC and 32% penetrates HOPG. The polarization parallel to the electrode surface was chosen partly because of past experience with solution scatterers (*29*) but principally to maintain the induced dipole axis perpendicular to the axis of the collection optics. Thus, the optical geometry corresponds to parallel polarization in the conventional Raman terminology. Based on results and theory for IR reflection/absorption spectroscopy (*28*), the normal Raman sampling depth and sensitivity may vary with incidence polarization, but these effects were not examined further in the present case.

The normal Raman spectra of various carbon electrode materials have been reported previously (*3*, *13*) and are relevant here only as initial spectra preceding Ag deposition. As expected, the cleaved HOPG and PG normal Raman spectra show minimal D band intensity due to their ordered structures, while for GC the D band is the most intense band observed. As noted in a previous report, polishing can affect the D/E_{2g} intensity ratio for GC, indicating that polishing affects several hundred angstroms of substrate near the surface (*30*).

The results support several useful conclusions about the SERS experiment following Ag deposition. First, Ag deposition on GC results in an up to 100-fold enhancement of the carbon Raman signal. Second, although the enhancement is always large, its magnitude is only semiquantitatively reproducible and strongly dependent upon deposition time and conditions. Third, the SERS enhancement is a maximum at an average Ag coverage of 0.21 mol/cm^2 for GC. This value corresponds to about 10–70 equivalent monolayers. Fourth, the Ag deposit occurs as 400–4000-Å particles, and the density and size distribution vary significantly with carbon substrate type and Ag deposition time. Fifth, the SERS enhancement

is large but fragile, with degradation of the effect occurring on a several minute time scale following Ag deposition.

Although the quantitative irreproducibility and instability of the SERS effect on carbon electrodes are problematic, the utility of the method is determined by conclusions about surface selectivity. In several of the cases examined, the SERS spectrum differs qualitatively from the normal Raman spectrum, in addition to being more intense. For polished GC, the D/E_{2g} intensity increases with Ag deposition, implying greater carbon disorder near the surface. For both cleaved PG and lightly polished HOPG, the D band intensity increased greatly with Ag deposition. Two explanations for these observations arise, both of which provide insight into the electrochemical consequences of carbon surface structure. First, the SERS enhancement length may be short enough (e.g., < 50 Å) to be more surface selective than normal Raman, thus revealing more surface defects or damage. For example, the polished surface of the GC should be more disordered than the bulk (*31*), and the SERS spectrum should exhibit a higher D band intensity. Similarly, lightly polished HOPG will be most disordered at its surface. The normal Raman spectrum of polished HOPG reveals no D band intensity because it samples >100 Å into the material, whereas the SERS spectrum reveals the D band and associated surface disorder. A second explanation of higher D band intensity is enhanced electrodeposition at surface defects, leading to Ag particles primarily at defects sites. On the basis of other redox systems, electron transfer to Ag^+ should be faster at edge plane defects than at the basal plane (*3, 13, 15*), and these defects will exhibit higher D band intensity. Such an effect has been proposed to explain Cu electrodeposition on GC, as observed by SEM (*31*). This hypothesis retains the surface selectivity mentioned earlier but further states that Ag deposition and accompanying enhanced Raman is selective for defect sites, particularly graphitic edges. The relative importance of general surface selectivity and selective defect enhancement may be carbon substrate dependent.

On the basis of the theory for the SERS enhancement factor, a rough estimate of the SERS sampling depth may be made. The enhancement factor (EF) is a maximum at the Ag particle surface, with its magnitude strongly dependent on particle shape and size (*16, 20, 32*). For Ag spheres and λ_L = 515 nm, the maximum enhancement on the Ag surface decreases rapidly as the radius increases above a few 100 Å. Of greater relevance to the current work is the dependence of EF on distance away from the Ag particle surface. There is general agreement that the EF is proportional to $(a/d)^{12}$, where a is the Ag sphere radius and d is the distance of a scatterer from the particle center (*16, 20*). Since the number of scatterers at a particular distance from a particle increases with d^2, the overall distance dependence of the Raman scattering becomes $(a/d)^{10}$. This prediction has been confirmed experimentally for polymer films deposited on Ag islands or Ag deposited on rough films (*20*).

The correlation of SERS intensity with the presence of small particles observed in the SEM's of Ag deposited on GC and HOPG confirms the importance of ca. 400-Å diameter particles for intense SERS. The 4000-Å particles observed on HOPG did not produce observable enhancement, and the Raman intensity roughly tracked the population of ca. 400-Å particles. Thus, it appears that the observed SERS effect is derived predominately from ca. 400-Å particles. For a = 200 Å, $(a/d)^{10}$ equals 0.38 for d = 220 Å and 0.11 for d = 250 Å. Thus, the Raman intensity has decreased by 62% when the scatterer is 20 Å from the surface of a 400-Å diameter Ag particle, and 89% at 50 Å away. These predictions are consistent with the 35–50-Å enhancement lengths observed by Murray and Allara for enhancement of a polymeric scatterer near rough Ag films (*20*). The predictions should only be considered as guides since the Ag particles cover a range of sizes and shapes, but a SERS sampling depth of a few tens of angstroms is consistent with both theory and experiment. The 25–50-Å enhancement length will be further decreased by the absorption of enhanced laser light and scattered photons by the carbon. For example, the product of $(a/d)^{10}$ and $\exp(-8\pi kz/\lambda)$ from eq 4 leads to a z_{63} sampling depth of 22 Å for a = 200 Å, d = 220 Å, and k = 0.70 and 20 Å for k = 1.52. Although approximate due to variations in Ag particle size, 20 Å is the best estimate of the SERS sampling depth, and is consistent with the estimate of Ishida et al. (*19*) for vapor-deposited Ag.

We have already seen the surface and defect selectivity of SERS over normal Raman for GC and polished HOPG. Figures 10 and 11 provide a further example of particular relevance to electrochemical effects of carbon surface structure. In Figure 10, it was clear that Ag deposition enhanced the D band scattering from cleaved PG. In Figure 11, the normal Raman spectrum of cleaved PG showed increased D intensity following Nd:YAG irradiation. The spectrum of Figure 11b indicates moderate disorder, with a microcrystallite size of ca 150 Å based on the D/E_{2g} intensity ratio (*33*). Upon Ag deposition, however, the D/E_{2g} ratio is much higher and the spectrum indicates much greater disorder. The normal Raman spectrum is probing at least 100 Å into the surface, and it has contributions from both the laser-damaged surface layer and undamaged substrate. Since the SERS experiment is more surface selective, the SERS spectrum reflects primarily the laser-damaged region near the surface. Apparently the laser damage depth is less than ~130 Å but deeper than the ~20-Å SERS sampling depth. These results indicate that normal Raman underestimates laser-induced surface damage because of insufficient surface selectivity. A examination of laser and electrochemically induced surface damage on HOPG will be presented later.

In summary, SERS following electrodeposition of Ag on carbon electrodes improves surface selectivity for Raman spectroscopy from a few hundred to a few tens of angstroms. Although the absolute SERS intensities vary significantly with conditions and time after deposition, changes in relative intensity and appearance of the spectrum can be useful for deducing surface structural features.

ACKNOWLEDGMENT

We thank Marc Porter and Darwin Popenoe of Iowa State University for providing the computer program to confirm the laser penetration depth.

Registry No. GC, 7440-44-0; PG, 7782-42-5; Ag, 7440-22-4; $NaClO_4$, 7601-89-0; $NaNO_3$, 7631-99-4.

LITERATURE CITED

(1) Kinoshita, K. *Carbon: Electrochemical and Physicochemical Properties*; Wiley: New York, 1988.
(2) Randin, J.-P. In *Encyclopedia of Electrochemistry of the Elements*; Bard, A. J., Ed.; Dekker: New York, 1976; Vol. 7, pp 1–291.
(3) McCreery, R. L. In *Electroanalytical Chemistry*; Bard, A. J., Ed.; Dekker: New York, 1991; Vol. 17.
(4) Stutts, K. J.; Kovach, P. M.; Kuhr, W. G.; Wightman, R. M. *Anal. Chem.* **1983**, *55*, 1632.
(5) Fagan, D. T.; Hu, I. F.; Kuwana, T. *Anal. Chem.* **1985**, *57*, 2759.
(6) Hu, I. F.; Kuwana, T. *Anal. Chem.* **1986**, *58*, 3235.
(7) Hu, I. F.; Karweik, D. H.; Kuwana, T. *J. Electroanal. Chem.* **1985**, *188*, 59.
(8) Rice, R. J.; Pontikos, N. M.; McCreery, R. L. *J. Am. Chem. Soc.* **1990**, *112*, 4617.
(9) Engstrom, R. C.; Strasser, V. A. *Anal. Chem.* **1984**, *56*, 136.
(10) Cabaniss, G. E.; Diamantis, A. A.; Murphy, W. R., Jr.; Linton, R. W.; Meyer, T. J. *J. Am. Chem. Soc.* **1985**, *107*, 1845.
(11) Kamau, G. N.; Willis, W. S.; Rusling, J. F. *Anal. Chem.* **1985**, *57*, 545.
(12) Thornton, D. C.; Corby, K. T.; Spendel, V. A.; Jordan, J.; Robbat, A.; Rutstrom, D. J.; Gross, M.; Ritzler, G. *Anal. Chem.* **1985**, *57*, 150.
(13) Bowling, R. J.; Packard, R. T.; McCreery, R. L. *J. Am. Chem. Soc.* **1989**, *111*, 1217.
(14) Bowling, R. J.; Packard, R. T.; McCreery, R. L. *Langmuir* **1989**, *5*, 683.
(15) Rice, R. J.; McCreery, R. L. *Anal. Chem.* **1989**, *61*, 1637.

(16) For reviews, see: (a) Chang, R. K.; Furtak, T. E. *Surface Enhanced Raman Scattering*; Plenum: New York, 1982. (b) Moskovits, M. *Rev. Mod. Phys.* **1985**, *57*, 783. (c) Chang, R. K.; Laube, B. L. *CRC Crit. Rev. Solid State Mater.* **1984**, *12*, 1.
(17) Pemberton, J. E. *J. Electroanal. Chem.* **1984**, *167*, 317.
(18) Davies, J. P.; Pachutta, S. J.; Cooks, R. G.; Weaver, M. J. *Anal. Chem.* **1986**, *58*, 1290.
(19) Ishida, H.; Fukuda, H.; Katagiri, G.; Ishitani, A. *Appl. Spectrosc.* **1986**, *40*, 322.
(20) Murray, C. A.; Allara, D. L. *J. Chem. Phys.* **1982**, *76*, 1290.
(21) Wang, Y.; McCreery, R. L. *Anal. Chem.* **1989**, *61*, 2647.
(22) Tindall, G. W.; Bruckenstein, S. *Electrochim. Acta* **1971**, *16*, 245.
(23) Wada, N.; Solin, S. *Physica* **1981**, *105B*, 353.
(24) Loudon, R. *J. Phys.* **1964**, *26*, 677.
(25) Loudon, R. *Adv. Phys.* **1964**, *13*, 423.
(26) Williams, M. W.; Arakawa, E. T. *J. Appl. Phys.* **1972**, *43*, 3460.
(27) Born, M.; Wolf, E. *Principles of Optics*; Pergamon: New York, 1959; pp 624–629.
(28) Porter, M. D.; Bright, T. B.; Allara, D. L.; Kuwana, T. *Anal. Chem.* **1986**, *58*, 2461.
(29) Packard, R. T.; McCreery, R. L. *J. Phys. Chem.* **1987**, *91*, 634.
(30) Rice, R.; Allred, C.; McCreery, R. L. *J. Electroanal. Chem.* **1989**, *263*, 163.
(31) Bodalbhai, L.; Brajter-Toth, A. *Anal. Chim. Acta* **1990**, *31*, 191.
(32) Zeman, E. J.; Schatz, G. C. *J. Phys. Chem.* **1987**, *91*, 634.
(33) Tuinstra, F.; Koenig, J. L. *J. Chem. Phys.* **1970**, *53*, 1126.

RECEIVED for review November 19, 1990. Accepted March 1, 1991. This work was supported primarily by the Surface and Analytical Chemistry division of the National Science Foundation. Laser activation and carbon surface modifications were developed under a grant from the Air Force Office of Scientific Research.

Lead-Selective Membrane Electrode Using Methylene Bis(diisobutyldithiocarbamate) Neutral Carrier

Satsuo Kamata* and Kazuhiro Onoyama

Faculty of Engineering, Kagoshima University, Korimoto, Kagoshima 890, Japan

Poly(vinyl chloride) membrane and membrane-coated carbon rod electrodes for lead(II) ion detection were developed by using the methylene and tetramethylene bis(diisobutyldithiocarbamate) neutral carriers and *o*-nitrophenyl octyl ether as a plasticizing solvent mediator. The membrane electrode based on methylene bis(diisobutyldithiocarbamate) exhibited good properties with a Nernstian slope of 28 mV/decade and linearity range of 10^{-2} to 10^{-6} M for the lead(II) ion. This membrane rejects alkali-metal ions by a factor of at least 10^2 and alkali-earth-metal ions by 10^5, although the copper(II) ion is not rejected.

The electrochemical properties and preparation of the lead(II) ion selective membrane electrodes have been studied by using active materials, one of which is the solid-state membranes made by sulfide, oxide, selenide, and other salts of lead together with silver sulfide (*1–13*) and the other is a liquid ion-exchange membrane (*14–17*). Recently, much interest has been paid to the ionophore ligands as sensing materials for neutral carrier type ion-selective electrodes due to the unique properties of the compounds. The ionophores with oxygen donor atoms have been usually studied for alkali- and alkali-earth-metal ion selective electrodes, and many selective ligands have been found for these metal ions (*18–23*). The lead ion selective electrodes were examined by using ionophores such as oxa- and dioxadicarbamides for PbX^+ ion determination (*24*) and dibenzo-18-crown-6 and its derivatives for Pb^{2+} ion determination (*25–27*), in which each ligand has oxygen donor atoms. It is well-known that the sulfur donor atom coordinates with transition-metal ions to form metal complexes. Several organosulfur compounds have been examined for copper(II) ion selective electrodes and have been shown to be useful copper(II) sensor materials (*28–32*). It is therefore expected that the sensitive ionophore ligands with sulfur donor atoms would also develop the lead ion-sensing materials, because it is possible to modify the ligand structure to improve ion selectivity.

In this paper, we report on a sensing system involving the lipophilic ionophores of methylene bis(diisobutyldithiocarbamate) (MBDiBDTC) and tetramethylene bis(diisobutyldithiocarbamate) (TMBDiBDTC) with *o*-nitrophenyl octyl ether (NPOE) as plasticizing solvent mediator by using two types of electrodes: conventional membrane electrodes and membrane-coated carbon rod electrodes. These new ionophores, each having different C-shaped cavities with four donor sulfur atoms, were expected to form selective complexes with transition-metal ions and to give an improved selectivity for the lead ion.

EXPERIMENTAL SECTION

Reagents and Chemicals. Poly(vinyl chloride) (PVC) and NPOE were obtained from Fluka (Buchs, Switzerland). Potassium tetrakis(*p*-chlorophenyl)borate (KTCPB) as an anion excluder was obtained from Dojin Kagaku (Kumamoto, Japan). Carbon rods were obtained from Nippon Carbon Co. (Yokohama, Japan). All solutions were prepared from analytical reagent grade salts with distilled, deionized water. All other materials and chemicals were of the best available laboratory reagent grade.

Preparation of MBDiBDTC and TMBDiBDTC. Diisobutylamine (0.14 mol) and 2-propanol (25 mL) were dissolved in water (300 mL) containing sodium hydroxide (0.14 mol). This mixture was stirred at room temperature, while carbon disulfide (0.14 mol) was slowly added to the solution and allowed to react for 2 h. The precipitate of sodium *N,N'*-diisobutyldithiocarbamate was filtered and crystallized from 2-propanol, yield 64%, mp 36–37 °C. The recrystallized sodium *N,N'*-diisobutyldithiocarbamate (0.05 mol) was dissolved in ethanol (300 mL), and methylene dibromide (0.025 mol) was added slowly to the solution with refluxing and stirring for 7 h. The final compound, MBDiBDTC, was obtained as white crystals and recrystallized from ethanol, yield 5.1 g, 60%, mp 69–70 °C. Anal. Calcd (found): H, 9.06 (9.05); C, 53.98 (53.96); N, 6.63 (6.65). IR (KBr), cm^{-1}: 740 (ν_{C-S-C}). NMR ($CDCl_3$), δ (ppm): 0.93 (d, 24 H), 2.33 (m, 4 H), 3.65 (d, 8 H), 5.40 (s, 2 H). TMBDiBDTC was synthesized by reacting sodium *N,N'*-diisobutyldithiocarbamate (0.04 mol)

0003-2700/91/0363-1295$02.50/0